Using coherent phonons for ultrafast control of the Dirac node of SrMnSb_{2}

Chris P. Weber, Madison G. Masten, Thomas C. Ogloza, Bryan S. Berggren, Michael K. L. Man, Keshav M. Dani, Jinyu Liu, Zhiqiang Mao, Dennis D. Klug, Adebayo A. Adeleke, and Yansun Yao

Phys. Rev. B **98**, 155115 — Published 8 October 2018

DOI: 10.1103/PhysRevB.98.155115

Using coherent phonons for ultrafast control of the Dirac node of $SrMnSb_2$

Chris P. Weber,[1,*] Madison G. Masten,[1] Thomas C. Ogloza,[1] Bryan S. Berggren,[1] Michael K. L. Man,[2] Keshav M. Dani,[2] Jinyu Liu,[3] Zhiqiang Mao,[3] Dennis D. Klug,[4] Adebayo A. Adeleke,[5] and Yansun Yao[5,†]

[1]*Department of Physics, Santa Clara University, 500 El Camino Real, Santa Clara, CA 95053-0315, USA*
[2]*Femtosecond Spectroscopy Unit, Okinawa Institute of Science and Technology Graduate University, 1919-1 Tancha, Onna-son, Kunigami, Okinawa 904-0495, Japan*
[3]*Department of Physics and Engineering Physics, Tulane University, New Orleans, Louisiana 70118, USA*
[4]*National Research Council of Canada, Ottawa, Canada K1A 0R6*
[5]*Department of Physics and Engineering Physics, University of Saskatchewan, Saskatoon, Saskatchewan, S7N 5E2, Canada*

(Dated: September 20, 2018)

$SrMnSb_2$ is a candidate Dirac semimetal, whose electrons near the Y point have the linear dispersion and low mass of a Dirac cone. Here we demonstrate that ultrafast, 800-nm optical pulses can launch coherent phonon oscillations in $Sr_{0.94}Mn_{0.92}Sb_2$, particularly an A_g mode at 4.4 THz. Through first-principles calculations of the electronic and phononic structure of $SrMnSb_2$, we show that high-amplitude oscillations of this mode would displace the atoms in a way that transiently opens and closes a gap at the node of the Dirac cone. The ability to control the nodal gap on a sub-picosecond timescale could create opportunities for the design and manipulation of Dirac fermions.

I. INTRODUCTION

Recent years have seen the proliferation of three-dimensional (3D) semimetals whose low-energy electron dispersions form linear Dirac cones crossing masslessly at a node.[1–4] These materials have garnered interest for their exotic photonic[5] and electronic[6] properties, and for their high mobility and large magnetoresistance.[6–8] Some possible technological uses, however, would require the opening of a gap at the node—for instance use in transistors[9] or in detection of dark matter.[10] Indeed, in the materials' 2D analog, graphene, several methods have been developed to control a gap.[9,11,12] It would be particularly desirable to be able to open and close a gap on ultrafast timescales. Such control could enable high-speed switching, or the investigation and tuning of electronic states beyond those available in static materials.

Experiments on the topological insulator Bi_2Se_3 have raised hope for the ultrafast control of Dirac nodes.[13] During illumination by a strong infrared pulse, Wang *et al.* demonstrated the creation of new nodes at the crossings of Floquet-Bloch sidebands, and used the light's polarization to open or close a gap at these nodes. It was subsequently proposed that ultrafast pulses can open a gap in graphene,[14] can convert a trivial insulator to a 3D Dirac semimetal[15] and *vice versa*, and can open[16] or close[17] a gap at the node of a Dirac semimetal. These proposed effects occur during the optical pulse, and require a strong electric field.

Incoherent, thermal phonons provide an alternate method for controlling Dirac nodes. Either raising or lowering the temperature may shift electronic bands, turning a trivial insulator into a topological insulator with surface Dirac states.[18] Phonons may break inversion symmetry, which has been proposed[19] to turn $NbNiTe_2$ into a Weyl semimetal. In the gapped Dirac semimetal $ZrTe_5$, Manzoni *et al.* saw that after photoexcitation, lattice heating caused the Dirac bands to shift by 60 meV within about 200 fs.[20] However, heat dissipates slowly—typically in nanoseconds—so that thermal approaches do not allow reversible, ultrafast control of Dirac cones.

Coherent phonons, however, overcome these difficulties. In a coherent phonon the atoms' positions oscillate in sync with each other, and the band structure follows[21–24]. Kim *et al.*[25] have proposed that oscillation of coherent phonons in topological crystalline insulators could lead to the formation of nontrivial topological phases, which would be evidenced in "flickering" surface-state Dirac cones. This proposal has not been experimentally realized, perhaps because the L-point, acoustic phonons required are difficult to coherently excite.

In this work we observe ultrafast excitation of a coherent phonon in $Sr_{0.94}Mn_{0.92}Sb_2$, a candidate Dirac semimetal, and identify the vibrational mode responsible, an A_g phonon that we name Mode 36. Our calculations on $SrMnSb_2$ show that this phonon could provide a route to the ultrafast control of the material's Dirac cone. We calculate that at high amplitudes Mode 36 will periodically open and close a gap at a Dirac node. This phonon-based control of the gap may be temporally separated from the photoexcited electrons and holes, may be started and stopped on a sub-picosecond timescale, and may reach high amplitudes even at low temperature.

A. $SrMnSb_2$

Calculations,[26,27] including ours, predict that $SrMnSb_2$ hosts Dirac-like bands near the Y-point, and that these bands have a gap of about 200 meV, but calculations disagree about where that gap lies relative to the Fermi level. Nonetheless, this gap has not been seen in photoemission[27] or magnetotransport,[28] because most samples are *p*-type. Experimentally, transport is dominated by Y-point carriers, despite the possibility of other bands intersecting the Fermi level. Y-point

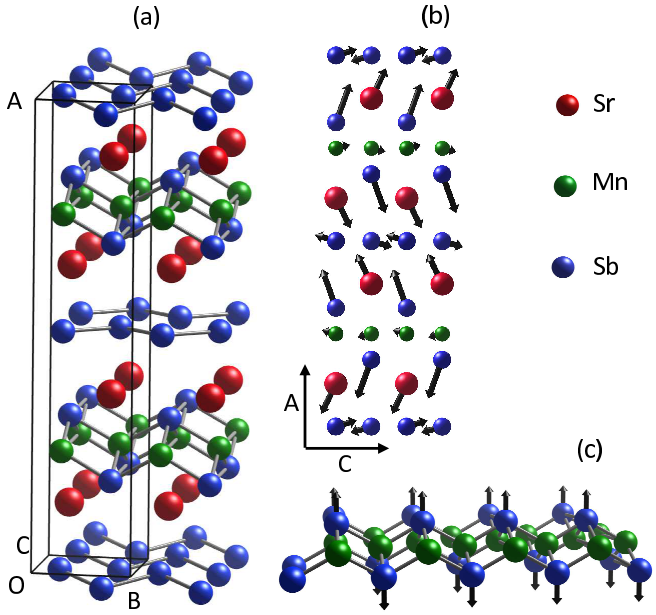

FIG. 1. (Color) **(a)** Crystal structure of $SrMnSb_2$, shown in a $1 \times 2 \times 2$ supercell. Sr, Mn and Sb atoms are shown in red, green and blue, respectively. A unit cell is outlined. **(b)** Illustration of how atoms are displaced by the structural distortion, viewed in the a-c plane. The lengths of arrows are exaggerated by a factor of 10. **(c)** Illustration of the main atomic displacements in phonon Mode 36. Only the Sb-Mn-Sb sandwich is shown.

carriers have a small Fermi surface, low effective mass, and steep dispersion—consistent only with a much smaller gap than predicted.[27,28] (Some indirect evidence for a gap may come from the optical conductivity of n-type samples.[29]) Experiments differ in measuring a trivial or a nontrivial Berry phase (with the nontrivial phase observed in measurements that extend to a Landau index of $n = 3$). Thus there remains uncertainty regarding both the possible topological nature and the possible gap of the Dirac cone near Y. It is not our purpose in this Article to resolve these questions, but to reveal a coherent phonon that may rapidly open or close that gap.

$SrMnSb_2$ preserves inversion symmetry but breaks time-reversal symmetry due to canted antiferromagnetic order. Its crystal structure [Fig. 1(a)] can be thought of in two parts: a plane of Mn sandwiched between Sb, and a square-net plane of Sb sandwiched between Sr. However, the material suffers a structural distortion [Fig. 1(b)] that renders it orthorhombic, distorts the Sb square net into zig-zag chains, and is responsible for the predicted gap near Y. The orthorhombic distortion makes $SrMnSb_2$ doubly promising for manipulation *via* coherent phonons. First, the connection between the distortion and a gap in the Dirac cone means that lattice motion is particularly apt to influence the nodal gap. Second, structurally distorted materials are particularly susceptible to the displacive excitation of coherent phonons:[21,30–33] their structural distortions are often driven by electronic energies that may be strongly modified by the absorption of an optical pulse.

II. METHODS

In the following we shall let the vector $\vec{Q}_{\rm orth}$ denote the positions of the 16 atoms in the unit cell of $SrMnSb_2$ (Appendix A 1). This structure belongs to point group D_{2h} and space group *Pnma* (#62). We let $\vec{Q}_{\rm tet}$ denote the hypothetical parent structure of tetragonal symmetry (D_{4h}, $P4/nmm$, #129). Mode 36, illustrated in Fig. 1(c), is a breathing mode that primarily moves the Sb atoms that surround the Mn plane, symmetrically towards and away from the plane. We will consider a "snapshot" of the structure during a high-amplitude oscillation in phonon Mode 36, denoted $\vec{Q}_{\rm orth} + 500\vec{M}_{36}$. Our approach—calculating the electronic dispersion for such snapshots of the crystal structure during a phonon oscillation—contrasts with the Floquet picture, which would treat the oscillations as a time-periodic Hamiltonian. Because the relevant phonon in $SrMnSb_2$ has just 18 meV, while the predicted gap at the Y-point is more than 10 times larger, we expect to obtain a good approximation of the dispersion, except possibly when the gap closes.[34]

Calculations of electronic structure were performed using the full-potential linearized augmented plane wave method *via* the WIEN2K code[35]. All calculations assume a G-type antiferromagnetic configuration for the ground state structure, and take into consideration spin-orbital coupling of Sb atoms. The on-site Coulomb interaction is treated with the Hubbard-U orbital correction level of theory with a $U - J$ value of 5 eV. 2000 k-points were employed in the sampling of the first Brillouin zone, for a k-mesh size of $4 \times 21 \times 21$ with an $RK_{\rm max}$ of 5.50.

Structural optimization and calculation of Raman and infrared frequencies were performed with the ABINIT code.[36,37] The Γ-point ($\vec{k} = 0$) phonon modes and corresponding displacement eignevectors of the 16-atom primitive orthorhombic cell were calculated with the linear response method employing the ABINIT program with a Troullier-Martins type norm-conserving pseudopotential (80 Ry for the kinetic energy cutoff).[38] The results were validated using the Vienna Ab-initio Simulation Package (VASP) code.[39] Full phonon calculations were performed to obtain thermal parameters for the displacement eigenvectors.

Mechanical stability was investigated by calculating the phonon dispersion relations in the whole Brillouin zone (Appendix A 2), using the density functional perturbation theory (DFPT), as implemented in VASP, using a $1 \times 4 \times 4$ supercell. Interpolation on the high-symmetry k-points was carried out using the PHONOPY program.[40] The interatomic force constants were calculated from the optimized supercell through the VASP package with a kinetic energy cutoff of 500 eV, on a $7 \times 7 \times 7$ k-point

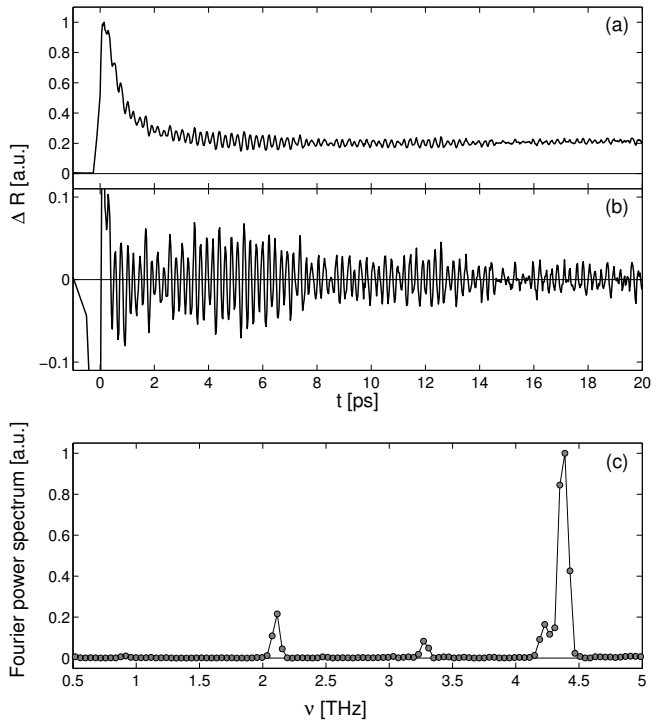

FIG. 2. **(a)**: Pump-probe signal measured at 10 K. Change in reflectance, ΔR, *vs.* probe delay t. **(b)**: The same data as in (a), but with the smooth part subtracted. **(c)**: Fourier power spectrum of signal.

mesh. A projector augmented wave potential[41] with the Perdew-Burke-Ernzerhof functional[42] was used. Convergence was achieved when the energy difference between two successive iterations was less than 10^{-6} eV/cell.

The samples of $Sr_{0.94}Mn_{0.92}Sb_2$ were grown using a self-flux method as detailed in Ref. 28. They had about 0.08 μ_B per Mn and a mobility near 10^4 cm^2/Vs. Shubnikov-de Haas oscillations on a sample from this batch had a frequency in the range of $66 - 70$ T, corresponding to a small, p-type Fermi surface with area $A_F = 0.64$ nm^{-2}. Ultrafast measurements used a mode-locked Ti:Sapphire laser operating at 800 nm and 80 MHz repetition rate, with a fluence near 10 μJ/cm^2. Measurements used standard chopping and lock-in detection, and were done in the transient-grating geometry of Ref. 43.

III. EXPERIMENTAL RESULTS

Our principal experimental finding is that excitation of $Sr_{0.94}Mn_{0.92}Sb_2$ by ultrafast laser pulses can coherently drive phonon oscillations in several modes, especially in Mode 36. Figure 2(a) shows how the reflectance of our sample changes, at 10 K, as a function of time after a laser pulse. The abrupt change in the reflectance, which decays within a few picoseconds, arises from the excitation and cooling of electrons and holes.[44] On top of this decay, oscillations are distinctly visible, as is beating between oscillation frequencies. (The oscillations also appear at room temperature, Appendix B 1.) The oscillation frequencies appear as peaks in the Fourier power spectrum in Fig. 2(c). The strongest oscillation is at 4.4 THz, near the frequency we predict for Mode 36. However, the close match between the measured and calculated frequency cannot be conclusive: the frequencies given by DFPT calculations are known to vary with computational methods.[45] Since $SrMnSb_2$ hosts 48 phonon modes, we need to consider the evidence more carefully before identifying our measured oscillation with Mode 36.

Mode #	Calculated frequency [THz]	Calculated Symmetry	Mode #	Calculated frequency [THz]	Calculated Symmetry
4	0.76	B_{3g}	30	3.52	A_g
5	0.82	A_g	32	3.86	A_g
15	2.04	A_g	36	4.36	A_g
20	2.62	B_{3g}	38	5.20	A_g
21	3.04	A_g	45	7.04	B_{3g}
26	3.24	B_{3g}	47	7.19	A_g

TABLE I. Phonon modes that may be visible in our measurements, with Γ-point frequencies from ABINIT. All 48 modes appear in the Supplemental Material.[45]

The vibrational frequencies observed in a pump-probe experiment correspond to Raman-active A_g and B_{3g} phonons, of which there are twelve. The Γ-point frequencies of these modes appear in Table I. There is a notable gap in frequencies around the 4.36 THz predicted for Mode 36. The closest frequency, that predicted for Mode 32, probably corresponds to a smaller peak seen in the Fourier spectrum, a "shoulder," at 4.2 THz.

Additionally, we can experimentally distinguish the A_g from the B_{3g} modes, through polarization-resolved spontaneous Raman scattering, shown in Appendix B 2. Finally, since the Mn moments in $Sr_{0.94}Mn_{0.92}Sb_2$ have a canted antiferromagnetic order, we ensure that the oscillation observed at 4.4 THz is a phonon and not a coherent magnon. We checked that its frequency does not shift in magnetic fields up to 17 T (Appendix B 1).

IV. THEORETICAL RESULTS

We now turn to calculations to learn what effect a high-amplitude motion of Mode 36 would have on the electronic structure. We note that, since our calculations occur on a finite mesh of k-points, we cannot say with certainty whether the gap closes completely; a Dirac node may appear gapless within our resolution even while a small avoided crossing remains. Nor do our methods allow the calculation of the topological invariant, if any, associated with a Dirac cone; typically a tight-binding model is used for this purpose.[19]

When there is no oscillation, $SrMnSb_2$ has the electronic structure of the orthorhombic crystal (Fig. 3, top), which is gapped throughout the Brillouin zone. By com-

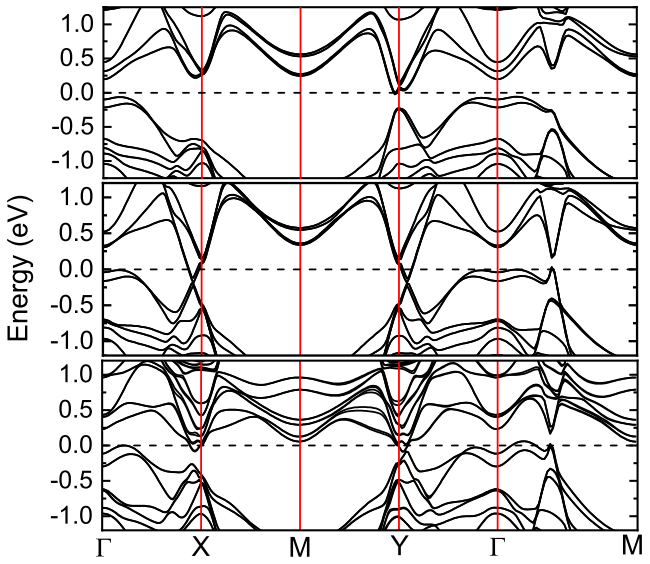

FIG. 3. (Color) **(Top)** Band structure for the equilibrium structure $\vec{Q}_{\rm orth}$. **(Middle)** Band structure for the parent structure $\vec{Q}_{\rm tet}$. **(Bottom)** Band structure for $\vec{Q}_{\rm orth}+500\vec{M}_{36}$.

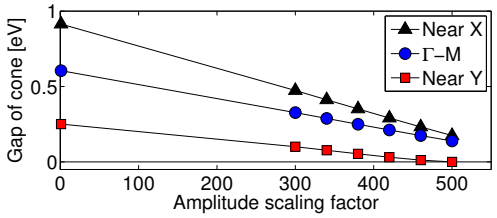

FIG. 4. (Color) Calculated gap vs. amplitude of atomic displacement along Mode 36.

parison, the tetragonal parent structure $\vec{Q}_{\rm tet}$ (which is not stable[26]) hosts three Dirac cones (Fig. 3, middle): a gapped cone on Γ-M, and cones near Y and near X that appear gapless, within our k-space resolution.

During a high-amplitude oscillation, the shift in the atoms' instantaneous position changes the electrons' instantaneous dispersion. Figure 3 (bottom) shows a snapshot of the band structure at $\vec{Q}_{\rm orth}+500\vec{M}_{36}$. Remarkably, the gap in the Dirac cone near Y appears closed. Indeed, as a function of the atomic displacement, the gap near Y narrows smoothly [Fig. 4] and closes at high oscillation amplitude. The critical amplitude is reached at $500\vec{M}_{36}$, when the Sb atoms surrounding the Mn plane have moved by 0.52 Å; this compares with a thermal motion at room temperature of 0.15 Å.[45] These calculations strongly suggest that, were one to drive a coherent, high-amplitude motion of $SrMnSb_2$ in Mode 36, one could periodically open and close a gap in the Dirac cone near the Y point. Displacements of this size should be experimentally feasible, as they have already been demonstrated in bismuth.[32]

Apart from Mode 36, we examined the effect of several other phonon modes on the electronic structure, including Mode 32, which at high amplitude would repair the zig-zag chains of Sb, rendering the Sb plane square. We found none that closes a gap in any of the Dirac cones; examples appear in Appendix A 3.

V. DISCUSSION AND CONCLUSIONS

Coherent phonons have already been observed in the 3D Dirac semimetal Cd_3As_2[46] and the type-II Weyl semimetal WTe_2.[47,48] Our work goes further by showing theoretically that the oscillation of a specific coherent phonon can control a gap at the Dirac node—which prior experiments had not suggested—and by experimentally identifying the desired phonon, Mode 36, as one readily excited by an optical pulse. This ready excitation is not wholly surprising: Mode 36 is predisposed to displacive, ultrafast excitation by its A_g symmetry and its strong overlap with the orthorhombic distortion. Neither, however, is it wholly expected: typically not all Raman-active modes appear in spontaneous Raman measurements, and even fewer appear as coherent phonons.

Prior theoretical work has proposed to control a Dirac node through phonons,[19,25] but without showing that the needed phonons may be controlled by ultrafast pulses, even in principle; some of the phonon modes are not Raman-active. Others have proposed to employ Floquet effects,[14–17] which rely on the periodic field of a light pulse—a sharply different mechanism lying well outside the adiabatic Born-Oppenheimer regime of our work. Our proposed use of a coherent phonon to control the Dirac node has several benefits. It may be less prone to damage the sample. The oscillation may be started by one laser pulse, and then either amplified or stopped by a subsequent pulse. (Experiments demonstrating this coherent control of the phonon will be reported elsewhere.) Finally, the oscillation may modulate the Dirac gap even after the photoexcited carriers have recombined. Indeed, the carriers' relaxation is known to be broadly similar across several 3D Dirac and Weyl semimetals:[20,43,44] the photoexcited electron and hole distribution, initially at high energy, thermalizes in much less than a picosecond, and subsequently cools in a few picoseconds. Since the period of Mode 36 is 0.23 ps, the electronic occupation becomes thermal within one or two oscillations. The coherent phonon, on the other hand, continues to oscillate for tens of picoseconds, allowing the possibility of controlling the Dirac gap after both the optical pulse and the electronic excitation are gone.

Before the ultrafast control of the Dirac node of $SrMnSb_2$ can be implemented, it will be important to directly observe the atomic displacements by ultrafast scattering[32] and the gap by ultrafast photoemission[21]—two techniques that recently have been successfully combined.[23] In addition to using more intense pump pulses, it may be advantageous to drive the oscillation

parametrically with a string of laser pulses spaced by the phonon period,[49] which can avoid pump-saturation effects and mitigate some mechanisms of sample damage and phonon anharmonicity. It is also desirable for both theory and experiment to clarify the size of the possible gap near the Y-point, the Dirac cone's possible topological nature, and the relation between as-grown samples of $Sr_{0.94}Mn_{0.92}Sb_2$ and the stoichiometric material, $SrMnSb_2$.

In conclusion, we have now shown that it should be possible to use a coherent phonon oscillation to periodically open and close a gap in the Y-point Dirac node of $SrMnSb_2$. We have identified the desired phonon, Mode 36. Experimentally, we have shown that coherent oscillations of Mode 36 are readily excited by optical pulses. The use of coherent phonons to control $SrMnSb_2$ thus benefits from a solid experimental foundation. It would allow sub-picosecond, on-and-off control of the Dirac node independently of photoexcited carriers, and could lead to new opportunities to study and manipulate 3D Dirac electrons.

ACKNOWLEDGMENTS

The authors thank S. Fahy, R. Flacau, D. E. Parker, and D. A. Reis for helpful conversations. This work was supported by the National Science Foundation DMR-1508278. Work at Tulane (sample growth) was supported by the U.S. Department of Energy under EPSCoR Grant No. DESC0012432, with additional support from the Louisiana Board of Regents.

Appendix A: Theory

1. Tables of crystal structure and phonon modes

In Table A.1 we detail the positions of the atoms $\vec{Q}_{\rm orth}$ in the unit cell of $SrMnSb_2$, along with two displacements that are important in this work: the orthorhombic distortion $\vec{Q}_{\rm dist} = \vec{Q}_{\rm orth} - \vec{Q}_{\rm tet}$, and the eigendisplacement in Mode 36, $\vec{M}_{36}$. The magnitude of $\vec{M}_{36}$ is chosen arbitrarily. As in the rest of this work the out-of-plane axis is a. (Though it is conventional to choose the c-axis out of plane, our choice is consistent with Refs. 26 and 28. Note that Fig. 1 of Ref. 26 uses a different axis convention from the rest of that work.) In the Supplemental Material,[45] we show the Γ-point frequencies, symmetries, and eigendisplacements for all 48 phonon modes. We also include, for selected temperatures, the elements of the thermal displacement tensors.

2. Phonon dispersion

The calculated phonon dispersion appears in Fig. A.1. The phonon dispersion has no negative frequencies, showing that the structure is stable. One feature that stands out in Fig. A.1 is the large density of phonon states near 2.2 THz, half the frequency of Mode 36. This density suggests that when Mode 36 is driven to high amplitude, a 4.4-THz phonon might readily decay, through anharmonic processes, into two 2.2-THz phonons. Fortunately, however, our experiments show little damping of Mode 36: at 10 K the oscillations remain visible up to 20 ps, and even at room temperature 14 oscillation cycles remain visible (see Fig. B.1).

Atom		Atomic coordinates [Å]			Orthorhombic distortion [Å]			Mode 36 displacement [fm]		
		x	y	z	Δx	Δy	Δz	Δx	Δy	Δz
1	Sr	2.60	1.09	3.21	0.19	0	-0.09	19	0	-6.3
2	Sr	7.83	3.26	1.01	-0.19	0	-0.09	-19	0	-6.3
3	Sr	18.26	3.26	1.19	-0.19	0	0.09	-19	0	6.3
4	Sr	13.02	1.09	3.39	0.19	0	0.09	19	0	6.3
5	Mn	5.24	1.09	1.01	0.02	0	-0.09	11	0	0.5
6	Mn	5.19	3.26	3.21	-0.02	0	-0.09	-11	0	0.5
7	Mn	15.62	3.26	3.38	-0.02	0	0.09	-11	0	-0.5
8	Mn	15.67	1.09	1.19	0.02	0	0.09	11	0	-0.5
9	Sb_p	0.04	1.09	0.97	0.04	0	-0.13	-0.7	0	15.1
10	Sb_{Mn}	6.43	1.09	3.21	-0.24	0	-0.09	103.4	0	0.5
11	Sb_p	10.39	3.26	3.17	-0.04	0	-0.13	0.7	0	15.1
12	Sb_{Mn}	4.00	3.26	1.01	0.24	0	-0.09	-103.4	0	0.5
13	Sb_p	-0.04	3.26	3.43	-0.04	0	0.13	0.7	0	-15.1
14	Sb_{Mn}	14.43	3.26	1.19	0.24	0	0.09	-103.4	0	-0.5
15	Sb_p	10.47	1.09	1.23	0.04	0	0.13	-0.7	0	-15.1
16	Sb_{Mn}	16.86	1.09	3.38	-0.24	0	0.09	103.4	0	-0.5

TABLE A.1. Coordinates of atoms in the unit cell of the crystal structure $\vec{Q}_{\rm orth}$. The subscripts "p" and "Mn" denote Sb atoms that form part of the square-net plane, or that sandwich the Mn plane, respectively. The directions x, y, and z correspond to crystal axes a, b, and c, respectively. The size of the unit cell is $20.86\mathring{A} \times 4.35\mathring{A} \times 4.39\mathring{A}$. Also shown are the shift $\vec{Q}_{\rm dist} = \vec{Q}_{\rm orth} - \vec{Q}_{\rm tet}$ due to the orthorhombic distortion, and the atoms' eigendisplacements in Mode 36.

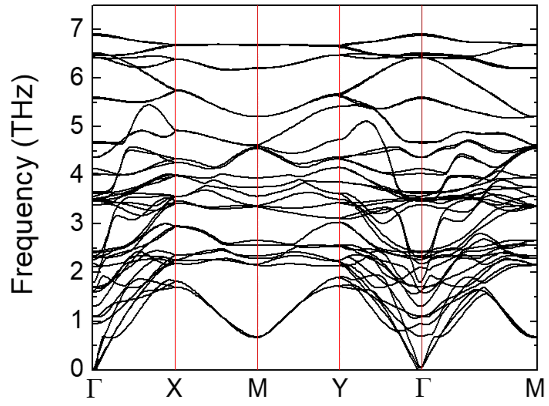

FIG. A.1. The phonon dispersion of the equilibrium (orthorhombic) structure $\vec{Q}_{\rm orth}$.

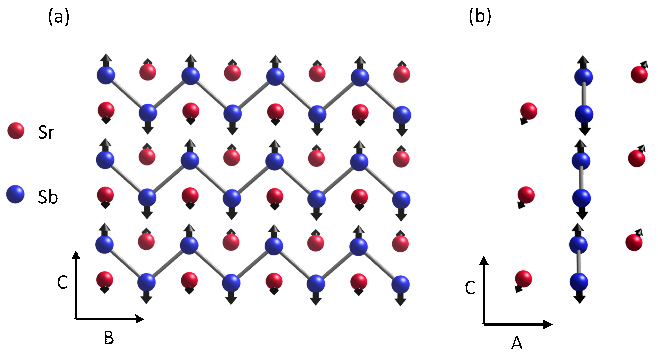

FIG. A.2. The larger atomic displacements in Mode 32, as viewed along (a) the a-axis or (b) the b-axis. The Sb plane is visible with its zig-zag chains, as are some of the Sr atoms adjacent to the plane. Other atoms move very little, and are omitted.

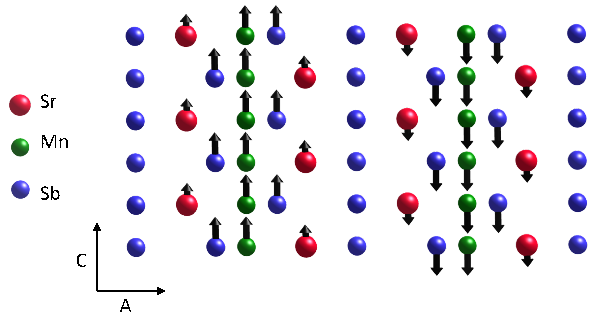

FIG. A.3. The larger atomic displacements in Mode 5, as viewed along the b-axis.

3. Examples of the effects of other phonon modes

It is natural to ask whether a coherent phonon vibration in any mode *other* than Mode 36 could also close the gap in any of the Dirac cones in $SrMnSb_2$—those near X, near Y, or along Γ-M. The presence of Dirac cones in the tetragonal structure $\vec{Q}_{\text{tet}}$ (Fig. 3(b)) suggests using a phonon parallel to the orthorhombic distortion—one with $\vec{M}_j \parallel \vec{Q}_{\text{dist}}$. At sufficiently high amplitude such a phonon would transiently reproduce the structure $\vec{Q}_{\text{tet}}$ and its electronic dispersion. However, for $SrMnSb_2$ no single mode matches $\vec{Q}_{\text{dist}}$; rather, the distortion is formed from a superposition of eight phonon modes (out of 48 total modes). All eight are Raman-active A_g modes.

Apart from Mode 36, we examined the effect of several of these phonon modes on the electronic structure. We found no other mode that closes the gap of a Dirac cone anywhere in the Brillouin zone. Here we present as examples the results for two modes of interest, Mode 32 and Mode 5. Both can be excited as coherent phonons that appear in our pump-probe data—Mode 32 as the "shoulder" below the 4.4-THz peak, and Mode 5 at around 0.9 THz [Fig. B.2(b)]. Mode 32, illustrated in Fig. A.2, consists primarily of c-axis motion of the Sb atoms that lie

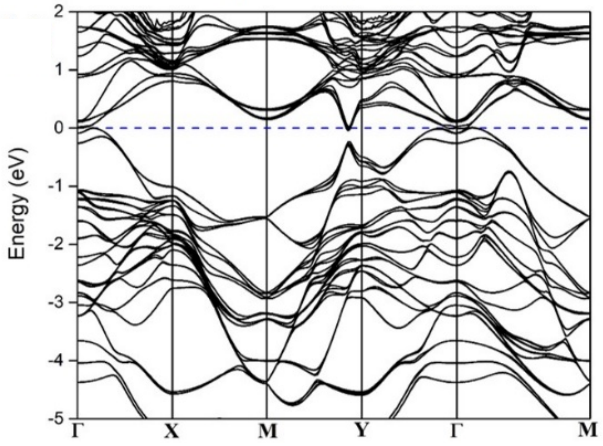

FIG. A.4. Band dispersion during a high-amplitude motion of Mode 32. The gap near the Y-point does not close.

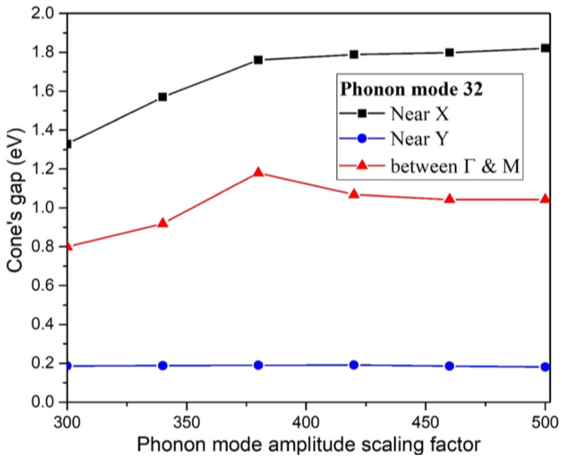

FIG. A.5. Gap *vs.* amplitude for Mode 32.

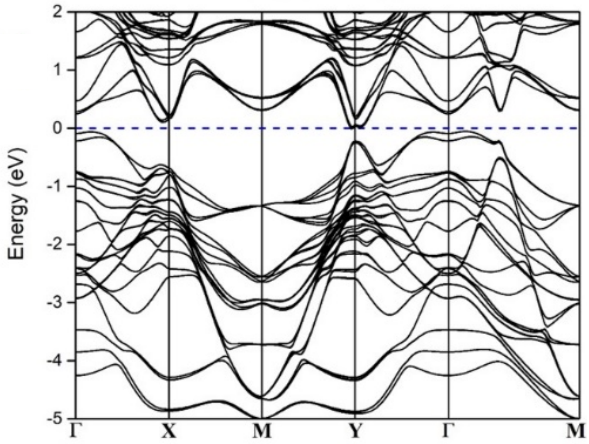

FIG. A.6. Band dispersion during a high-amplitude motion of Mode 5. The gap near the Y-point does not close.

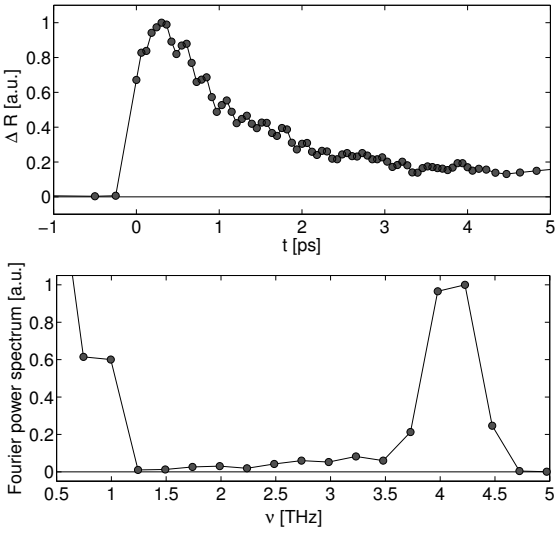

FIG. B.1. (a) Pump-probe signal at room temperature. (b) FFT of the room-temperature data.

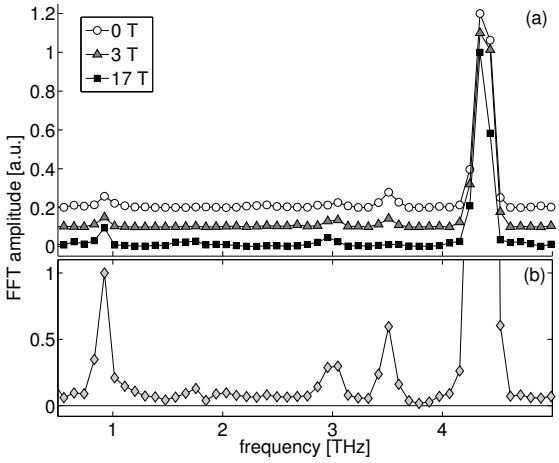

FIG. B.2. (a) Fourier-transform of pump-probe data at selected fields. Shifted vertically for clarity. (b) Average FFT of eight data sets measured at magnetic fields varying from 0 T to 17 T.

in the Sb plane; at high amplitude it would periodically repair the zig-zag chains of Sb, rendering the Sb plane square. (It moves other atoms, notably the Sr, but by lesser amounts.) Mode 5, illustrated in Fig. A.3, consists primarily of a shearing motion, along the c axis, of the Sb-Mn-Sb sandwiches.

Figures A.4 and A.5 show the effect of a large motion of Mode 32 on the electronic structure. The snapshot in Fig. A.4 is for an amplitude of 420, which corresponds to moving the in-plane Sb atoms by 0.37 Å, and the Sr atoms by 0.27 Å. The Dirac cone near the Y-point remains gapped, as indeed it does for both smaller and larger displacements along Mode 32 (Fig. A.5). Similar data appear in Fig. A.6 for Mode 5 at an amplitude of 300. This amplitude corresponds to moving the Mn atoms by 0.24 Å, and the Sb atoms that are near the Mn by 0.23 Å.

Appendix B: Experiment

1. Additional pump-probe data

Figure B.1(a) shows pump-probe data at room temperature, which exhibit coherent oscillations. The peak in their Fourier transform around 4.4 THz [Fig. B.1(b)] shows that the oscillation of Mode 36 is prominent at room temperature, as it is at low temperature. It is possible, but not certain, that the oscillation may "soften" slightly with temperature, shifting its frequency below 4.4 THz. Though the room-temperature oscillations damp more rapidly than at low temperature—they are nearly gone by 4 ps—nonetheless 14 oscillation cycles remain visible. We did not collect data past 4 ps, which is why the frequency-resolution of the Fourier transform is low.

To confirm that the low-temperature oscillations at 4.4 THz are associated with a phonon, and not with a magnon, we measured pump-probe data as a function of a magnetic field applied along the out-of-plane axis (the a-axis). We kept the sample at 15 K, and used a frequency-doubled fiber laser at 810 nm with a pulse duration of 140 fs and 2 nJ per pulse. Figure B.2(a) shows that, as expected for a phonon, the 4.4-THz peak does not shift its frequency measurably at fields up to 17 T.

The pump-probe setup in the magnet offered limited signal-to-noise, so we could not conclusively determine whether oscillations at frequencies other than 4.4 THz might shift their frequencies with magnetic field. However, Fig. B.2(b) shows the average of our magnetic-field data, allowing a closer look at these smaller peaks. The oscillation at 0.9 THz that appears in these data also appears, though less prominently, in the zero-field pump-probe data taken using a Ti:Sapphire laser.

2. Spontaneous Raman measurements

We can experimentally distinguish the A_g from the B_{3g} modes, through polarization-resolved spontaneous Raman scattering,[50,51] thereby supporting our identification of the observed 4.4-THz oscillations with Mode 36. Here we provide details of those measurements and their analysis.

The Raman measurements used a Tokyo Instruments NanoFinder micro-Raman spectrometer with a 532 nm laser source. The polarization of the incident light was fixed, and we used a polarizer to select scattered light polarized either parallel or perpendicular to the incident polarization. The sample was kept at room temperature, and was rotated about the incident axis (the a-axis) through an angle θ, with $\theta = 0$ chosen arbitrarily (illus-

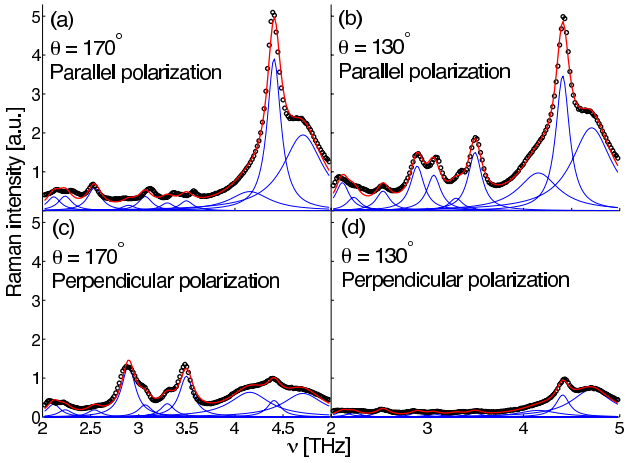

FIG. B.3. Examples of Raman data measured as a function of light polarization and sample rotation θ. Circles: measured data. Red line: fit of data to a sum of ten Lorentzian peaks. Blue lines: the individual Lorentzian peaks used in each fit.

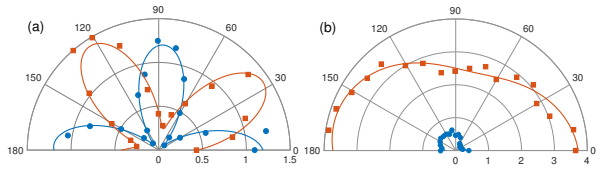

FIG. B.4. (Color) Polar plots of the Raman strength (in arbitrary units) of two representative phonon modes, 3.5 THz **(a)** and 4.4 THz **(b)**, as a function of sample rotation θ. Squares (circles) represent the scattered signal for light polarized parallel (perpendicular) to the incident light. The contrast between these two peaks' angle-dependence illustrates the ability to distinguish B_{3g} from A_g phonons through Raman measurements.

trated in the Supplemental Material[45]). Because some twinning of the sample was visible, after each rotation we returned to measuring the same spot. (However, a few checks of other spots showed that the twinning did not appear to have a large effect on the Raman signal.) As is expected, not all twelve A_g and B_{3g} modes appear in the Raman data, and the peaks' relative magnitudes differ from those seen in the ultrafast measurements.[30,31,33]

To analyze the Raman spectra we fit the data to ten Lorentzian peaks (Fig. B.3). With the exception of two with widths of 0.5 THz, the peaks' widths were fixed to our experimental resolution of 0.16 THz (full widths at half-max). We used fits to angle- and polarization-integrated data to determine peak positions. Subsequently, in fitting angle- and polarization-resolved data, the positions and widths were fixed, and only the peaks' amplitudes were allowed to vary.

Figure B.3 shows examples of the data and fits for two angles. The fits match the data well, particularly for the larger peaks. The symmetries of some peaks are readily apparent in the data. For the peak at 4.4 THz, the parallel-polarized signal is always large, and the perpendicularly-polarized signal is always small, regardless of θ; this is the behavior expected of an A_g mode. In contrast, the peaks near 2.8 THz and 3.5 THz behave as expected of B_{3g} modes: they give a maximal parallel-polarized signal at $\theta = 130°$, but when the sample is rotated nearly 45° from that angle they give a minimal parallel-polarized signal, and a maximal signal for perpendicular polarization. For some smaller peaks, however, the fits appeared to allow cross-talk between their amplitudes and those of their larger neighbors, leaving their symmetries less well-determined.

Figures B.4(a) and B.4(b) show the magnitudes of two representative peaks as a function of θ. The peak at 3.5 THz shows the distinctive daisy shape characteristic of B_{3g} modes, while the peak at 4.4 THz has a nearly isotropic shape that identifies it as A_g, strengthening its identification with Mode 36.

* cweber@scu.edu
† yansun.yao@usask.ca

[1] A. A. Burkov, M. D. Hook, and L. Balents, Phys. Rev. B **84**, 235126 (2011).
[2] X. Wan, A. M. Turner, A. Vishwanath, and S. Y. Savrasov, Phys. Rev. B **83**, 205101 (2011).
[3] S. M. Young, S. Zaheer, J. C. Y. Teo, C. L. Kane, E. J. Mele, and A. M. Rappe, Phys. Rev. Lett. **108**, 140405 (2012).
[4] H. Weng, C. Fang, Z. Fang, B. A. Bernevig, and X. Dai, Phys. Rev. X **5**, 011029 (2015).
[5] L. Wu, S. Patankar, T. Morimoto, N. L. Nair, E. Thewalt, A. Little, J. G. Analytis, J. E. Moore, and J. Orenstein, Nat. Phys. **13**, 350 (2017).
[6] X. Huang, L. Zhao, Y. Long, P. Wang, D. Chen, Z. Yang, H. Liang, M. Xue, H. Weng, Z. Fang, X. Dai, and G. Chen, Phys. Rev. X **5**, 031023 (2015).
[7] T. Liang, Q. Gibson, M. N. Ali, M. Liu, R. J. Cava, and N. P. Ong, Nat. Mater. **14**, 280 (2015).
[8] C. Shekhar, A. K. Nayak, Y. Sun, M. Schmidt, I. Nicklas, M. Leermakers, U. Zeitler, Y. Skourski, J. Wosnitza, Z. Liu, Y. Chen, W. Schnelle, H. Borrmann, Y. Grin, C. Felser, and B. Yan, Nat. Phys. **11**, 645 (2015).
[9] F. Xia, D. B. Farmer, Y.-m. Lin, and P. Avouris, Nano Lett. **10**, 715 (2010).
[10] Y. Hochberg, Y. Kahn, M. Lisanti, K. M. Zurek, A. G. Grushin, R. Ilan, S. M. Griffin, Z.-F. Liu, S. F. Weber, and J. B. Neaton, Phys. Rev. D **97**, 015004 (2018).
[11] Y. Zhang, T.-T. Tang, C. Girit, Z. Hao, M. C. Martin, A. Zettl, M. F. Crommie, Y. R. Shen, and F. Wang, Nature (London) **459** (2009).
[12] M. S. Nevius, M. Conrad, F. Wang, A. Celis, M. N. Nair, A. Taleb-Ibrahimi, A. Tejeda, and E. H. Conrad, Phys. Rev. Lett. **115**, 136802 (2015).
[13] Y. H. Wang, H. Steinberg, P. Jarillo-Herrero, and N. Gedik, Science **342**, 453 (2013).

[14] M. A. Sentef, M. Claassen, A. F. Kemper, B. Moritz, T. Oka, J. K. Freericks, and T. P. Devereaux, Nat. Commun. **6** (2015).
[15] A. Narayan, Phys. Rev. B **91**, 205445 (2015).
[16] H. Hübener, M. A. Sentef, U. De Giovannini, A. F. Kemper, and A. Rubio, Nat. Commun. **8** (2017).
[17] O. V. Kibis, K. Dini, I. V. Iorsh, and I. A. Shelykh, Phys. Rev. B **95**, 125401 (2017).
[18] G. Antonius and S. G. Louie, Phys. Rev. Lett. **117**, 246401 (2016).
[19] L.-L. Wang, N. H. Jo, Y. Wu, Q. S. Wu, A. Kaminski, P. C. Canfield, and D. D. Johnson, Phys. Rev. B **95**, 165114 (2017).
[20] G. Manzoni, A. Sterzi, A. Crepaldi, M. Diego, F. Cilento, M. Zacchigna, P. Bugnon, H. Berger, A. Magrez, M. Grioni, and F. Parmigiani, Phys. Rev. Lett. **115**, 207402 (2015).
[21] F. Schmitt, P. S. Kirchmann, U. Bovensiepen, R. G. Moore, L. Rettig, M. Krenz, J.-H. Chu, N. Ru, L. Perfetti, D. H. Lu, M. Wolf, I. R. Fisher, and Z.-X. Shen, Science **321**, 1649 (2008).
[22] J. A. Sobota, S.-L. Yang, D. Leuenberger, A. F. Kemper, J. G. Analytis, I. R. Fisher, P. S. Kirchmann, T. P. Devereaux, and Z.-X. Shen, Phys. Rev. Lett. **113**, 157401 (2014).
[23] S. Gerber, S.-L. Yang, D. Zhu, H. Soifer, J. A. Sobota, S. Rebec, J. J. Lee, T. Jia, B. Moritz, C. Jia, A. Gauthier, Y. Li, D. Leuenberger, Y. Zhang, L. Chaix, W. Li, H. Jang, J.-S. Lee, M. Yi, G. L. Dakovski, S. Song, J. M. Glownia, S. Nelson, K. W. Kim, Y.-D. Chuang, Z. Hussain, R. G. Moore, T. P. Devereaux, W.-S. Lee, P. S. Kirchmann, and Z.-X. Shen, Science **357**, 71 (2017).
[24] J. Weisshaupt, A. Rouzée, M. Woerner, M. J. J. Vrakking, T. Elsaesser, E. L. Shirley, and A. Borgschulte, Phys. Rev. B **95**, 081101(R) (2017).
[25] J. Kim and S.-H. Jhi, Phys. Rev. B **92**, 125142 (2015).
[26] M. A. Farhan, G. Lee, and J. H. Shim, J. Phys.: Cond. Mat. **26**, 042201 (2014).
[27] S. V. Ramankutty, J. Henke, A. Schiphorst, R. Nutakki, S. Bron, G. Araizi-Kanoutas, S. K. Mishra, L. Li, Y. K. Huang, T. K. Kim, M. Hoesch, C. Schlueter, T.-L. Lee, A. de Visser, Z. Zhong, J. van Wezel, E. van Heumen, and M. S. Golden, SciPost Phys. **4**, 010 (2018).
[28] J. Y. Liu, J. Hu, Q. Zhang, D. Graf, H. B. Cao, S. M. A. Radmanesh, D. J. Adams, Y. L. Zhu, G. F. Cheng, X. Liu, W. A. Phelan, J. Wei, M. Jaime, F. Balakirev, D. A. Tennant, J. F. DiTusa, I. Chiorescu, L. Spinu, and Z. Q. Mao, Nat. Mater. **16**, 905 (2017).
[29] H. J. Park, L. J. Sandilands, J. S. You, H. S. Ji, C. H. Sohn, J. W. Han, S. J. Moon, K. W. Kim, J. H. Shim, J. S. Kim, and T. W. Noh, Phys. Rev. B **93**, 205122 (2016).
[30] T. K. Cheng, S. D. Brorson, A. S. Kazeroonian, J. S. Moodera, G. Dresselhaus, M. S. Dresselhaus, and E. P. Ippen, Appl. Phys. Lett. **57**, 1004 (1990).
[31] H. J. Zeiger, J. Vidal, T. K. Cheng, E. P. Ippen, G. Dresselhaus, and M. S. Dresselhaus, Phys. Rev. B **45**, 768 (1992).
[32] K. Sokolowski-Tinten, C. Blome, J. Blums, A. Cavalleri, C. Dietrich, A. Tarasevitch, I. Uschmann, E. Förster, M. Kammler, M. Horn-von Hoegen, and D. von der Linde, Nature **422**, 287 (2003).
[33] J. J. Li, J. Chen, D. A. Reis, S. Fahy, and R. Merlin, Phys. Rev. Lett. **110**, 047401 (2013).
[34] S. Pisana, M. Lazzeri, C. Casiraghi, K. S. Novoselov, A. K. Geim, A. C. Ferrari, and F. Mauri, Nat. Mater. **6**, 198 (2007).
[35] P. Blaha, K. Schwarz, G. Madsen, D. Kvasnicka, and J. Luitz, WIEN2K, an augmented plane wave + local orbitals program for calculating crystal properties (2001).
[36] X. Gonze, B. Amadon, P.-M. Anglade, J.-M. Beuken, F. Bottin, P. Boulanger, F. Bruneval, D. Caliste, R. Caracas, M. Côté, T. Deutsch, L. Genovese, P. Ghosez, M. Giantomassi, S. Goedecker, D. R. Hamann, P. Hermet, F. Jollet, G. Jomard, S. Leroux, M. Mancini, S. Mazevet, M. J. T. Oliveira, G. Onida, Y. Pouillon, T. Rangel, G.-M. Rignanese, D. Sangalli, R. Shaltaf, M. Torrent, M. J. Verstraete, G. Zerah, and J. W. Zwanziger, Comput. Phys. Commun. **180**, 2582 (2009).
[37] A. Palaria, X. Wang, B. P. Haley, M. Mannino, and G. Klimeck, ABINIT (2008), doi:10.4231/D30G3H028, https://nanohub.org/resources/ABINIT.
[38] N. Troullier and J. L. Martins, Phys. Rev. B **43**, 1993 (1991).
[39] G. Kresse and J. Hafner, Phys. Rev. B **47**, 558 (1993).
[40] A. Togo and I. Tanaka, Scripta Mater. **108**, 1 (2015).
[41] G. Kresse and D. Joubert, Phys. Rev. B **59**, 1758 (1999).
[42] J. P. Perdew, K. Burke, and M. Ernzerhof, Phys. Rev. Lett. **77**, 3865 (1996).
[43] C. P. Weber, E. Arushanov, B. S. Berggren, T. Hosseini, N. Kouklin, and A. Nateprov, Appl. Phys. Lett. **106**, 231904 (2015).
[44] C. P. Weber, B. S. Berggren, M. G. Masten, T. C. Ogloza, S. Deckoff-Jones, J. Madéo, M. K. L. Man, K. M. Dani, L. Zhao, G. Chen, J. Liu, Z. Mao, L. M. Schoop, B. V. Lotsch, S. S. P. Parkin, and M. Ali, J. Appl. Phys. **122**, 223102 (2017).
[45] See Supplemental Material at [URL will be inserted by publisher] for the frequencies, symmetries, and eigendisplacements of all phonon modes, for the atoms' thermal displacement tensors, and for additional experimental and theoretical details.
[46] F. Sun, Q. Wu, Y. L. Wu, H. Zhao, C. J. Yi, Y. C. Tian, H. W. Liu, Y. G. Shi, H. Ding, X. Dai, P. Richard, and J. Zhao, Phys. Rev. B **95**, 235108 (2017).
[47] Y. M. Dai, J. Bowlan, H. Li, H. Miao, S. F. Wu, W. D. Kong, Y. G. Shi, S. A. Trugman, J.-X. Zhu, H. Ding, A. J. Taylor, D. A. Yarotski, and R. P. Prasankumar, Phys. Rev. B **92**, 161104(R) (2015).
[48] B. He, C. Zhang, W. Zhu, Y. Li, S. Liu, X. Zhu, X. Wu, X. Wang, H.-H. Wen, and M. Xiao, Sci. Rep. **6**, 30487 (2016).
[49] L. Dhar, J. A. Rogers, and K. A. Nelson, Chem. Rev. **94**, 157 (1994).
[50] H. Liu, P. Richard, L. X. Zhao, G.-F. Chen, and H. Ding, J. Phys.: Cond. Mat. **28**, 295401 (2016).
[51] Q. Song, X. Pan, H. Wang, K. Zhang, Q. Tan, P. Li, Y. Wan, Y. Wang, X. Xu, M. Lin, X. Wan, F. Song, and L. Dai, Sci. Rep. **6**, 29254 (2016).